Tests and applications of self-consistent cranking in the interacting boson model

Serdar Kuyucak*

*Department of Theoretical Physics, Research School of Physical Sciences, Australian National University,
Canberra, ACT 0200, Australia*

Michiaki Sugita†

Japan Atomic Energy Research Institute, Tokai, Ibaraki 319-11, Japan

The self-consistent cranking method is tested by comparing the cranking calculations in the interacting boson model with the exact results obtained from the SU(3) and O(6) dynamical symmetries and from numerical diagonalization. The method is used to study the spin dependence of shape variables in the sd and sdg boson models. When realistic sets of parameters are used, both models lead to similar results: axial shape is retained with increasing cranking frequency while fluctuations in the shape variable γ are slightly reduced.
[S0556-2813(99)05206-1]

PACS number(s): 21.60.Ev, 21.60.Fw

I. INTRODUCTION

Self-consistent cranking (SCC) is one of the most popular methods to study collective rotations in nuclear many-body systems [1]. Within the Hartree-Fock framework, it has provided important insights into the backbending phenomena, and currently, it is being used actively in studies of superdeformed nuclei [2]. In stark contrast, it has been rarely used in the interacting boson model (IBM) [3]. In fact, there is only one application of SCC to IBM where a study of moment of inertia (MOI) is carried out [4]. In the early stages of the model, an obvious reason for this neglect was the availability of exact results (either via dynamical symmetries or numerical diagonalization), which left little room for development of approximate methods such as SCC. In later extensions of the IBM (e.g., sdg-IBM), dynamical symmetries were not very useful, and numerical diagonalization could not be carried out due to large basis space, hence alternative methods were needed. At around the same time, however, an exact angular momentum projection technique was developed for axially symmetric boson systems ($1/N$ expansion [5]), which provided analytical solutions for general Hamiltonians in large basis spaces, filling the gap left by the other methods. Although the assumption of axial symmetry is reasonable for most deformed nuclei in their ground states, triaxial effects are known to play a role, especially at high spins [6]. Therefore a study of the evolution of shapes in the IBM would be useful in order to investigate such questions as the effects of triaxiality in nuclear spectra, ways of incorporating it in the IBM Hamiltonian, and whether an improved description of spectra can be obtained if triaxial effects are taken into account.

In this paper, we first present tests of the SCC by comparing the cranking calculations with the exact results obtained in the SU(3) and O(6) limits, as well as from diagonalization of more realistic Hamiltonians in the sd-IBM. The SCC method is then used in a study of triaxiality in the IBM both in the sd- and sdg-boson versions of the model.

II. CRANKING FORMALISM IN THE IBM

The SCC in the IBM was formulated in Ref. [4] to which we refer for details, especially concerning the construction of the intrinsic state and the symmetries it possesses. For a given IBM Hamiltonian H and intrinsic state $|N,\mathbf{x}\rangle$, the SCC around the x axis is described by

$$\delta\langle N,\mathbf{x}|H-\omega\hat{L}_x|N,\mathbf{x}\rangle=0, \tag{1}$$

where $\hat{L}_x$ is the x component of the angular momentum operator, N is the boson number and $\mathbf{x}$ are the variational parameters to be determined from the extremum condition. For convenience, we consider a general formulation of the IBM which will be tailored to specific cases later. Thus, we introduce the boson creation and annihilation operators $b^\dagger_{l\mu},b_{l\mu}$ with $l=0,2,4,\ldots$, where $b_0=s$, $b_2=d$, $b_4=g$, etc. The intrinsic state is given by a condensate of intrinsic bosons as

$$|N,\mathbf{x}\rangle=(N!)^{-1/2}(b^\dagger)^N|0\rangle, \quad b^\dagger=\sum_l\sum_{m=-l}^l x_{lm}b^\dagger_{lm}, \tag{2}$$

where x_{lm} are the normalized boson mean fields, i.e., $\mathbf{x}\cdot\mathbf{x}=1$. Due to the symmetries in the cranked system [4], x_{lm} are real and $x_{l-m}=x_{lm}$. Note that the odd-m components of x_{lm} vanish in the static limit ($\omega=0$), but not in general. Thus, invoking the normalization condition (e.g., setting $x_{00}=1$), there are three independent variational parameters in the sd-IBM (x_{20},x_{21},x_{22}) and five more in the sdg-IBM ($x_{40},\ldots,x_{44}$). For the IBM Hamiltonian, we use the generic multipole form

$$H=\sum_l\varepsilon_l\hat{n}_l-\sum_{k=0}^{2l_{max}}\kappa_k T^{(k)}\cdot T^{(k)}, \tag{3}$$

*Electronic address: sek105@rsphysse.anu.edu.au
†Deceased.

where the boson number and multipole operators are given by

$$\hat{n}_l = \sum_\mu b_{l\mu}^\dagger b_{l\mu}, \quad T_\mu^{(k)} = \sum_{jl} t_{kjl} [b_j^\dagger \tilde{b}_l]_\mu^{(k)}. \quad (4)$$

In particular, the angular momentum operators are

$$\hat{L}_x = \frac{-1}{\sqrt{2}} (\hat{L}_{+1} - \hat{L}_{-1}),$$

$$\hat{L}_\mu = \sum_l \sqrt{l(l+1)(2l+1)/3} [b_l^\dagger \tilde{b}_l]_\mu^{(1)}. \quad (5)$$

The parameters of the Hamiltonian consist of the single boson energies, ε_l, the multipole coupling strengths κ_k, and the multipole parameters t_{kjl}. The Hermiticity condition on multipole operators requires that $t_{kjl} = t_{klj}$.

The expectation values in Eq. (3) can be evaluated in a straightforward manner using boson calculus techniques. For the one-body operators, one simply obtains

$$\langle N, \mathbf{x} | \hat{n}_l | N, \mathbf{x} \rangle = N \sum_m \frac{x_{lm}^2}{\mathbf{x} \cdot \mathbf{x}}. \quad (6)$$

Calculations for the multipole interactions are somewhat more involved but the expectation values can again be reduced to a compact form

$$\langle N, \mathbf{x} | T^{(k)} \cdot T^{(k)} | N, \mathbf{x} \rangle = N(N-1) \sum_{\mu=-k}^k (-1)^\mu A_{k\mu} A_{k-\mu}$$

$$+ N \sum_{lm} \varepsilon_l' \frac{x_{lm}^2}{\mathbf{x} \cdot \mathbf{x}}. \quad (7)$$

Here $A_{k\mu}$ corresponds to the expectation value of the operator $T_\mu^{(k)}$ in a single boson state and is given by

$$A_{k\mu} = \sum_{jnlm} (-1)^m \langle jnlm | k\mu \rangle t_{kjl} \frac{x_{jn}x_{lm}}{\mathbf{x} \cdot \mathbf{x}}. \quad (8)$$

Using the symmetries imposed on the mean fields and the Hermiticity condition, it can be shown that $A_{k\mu}$ vanishes if $k + \mu$ is odd, and furthermore $A_{k-\mu} = (-1)^k A_{k\mu}$. Thus, for even multipoles, only the positive, even μ values contribute to the sum in Eq. (7). The second term in Eq. (7) arises from the normal ordering of the boson operators and corresponds to an effective one-body term with boson energies

$$\varepsilon_l' = \frac{2k+1}{2l+1} \sum_j t_{kjl}^2. \quad (9)$$

Finally, the expectation value of $\hat{L}_x$ is

$$\langle N, \mathbf{x} | \hat{L}_x | N, \mathbf{x} \rangle = -N \sum_{lmn} (-1)^m$$

$$\times \langle lnl-m | 11 \rangle \sqrt{2l(l+1)(2l+1)/3}$$

$$\times \frac{x_{ln}x_{lm}}{\mathbf{x} \cdot \mathbf{x}}. \quad (10)$$

For a given angular frequency ω, the cranking equation (1) is solved numerically by minimizing the cranking expression $E(\mathbf{x}, \omega) = \langle H - \omega L_x \rangle$ with respect to the mean fields $\mathbf{x}$. The dynamical MOI is calculated from the derivative of $\langle \hat{L}_x \rangle$, Eq. (10) as [7]

$$\mathcal{J}^{(2)} = \frac{d\langle \hat{L}_x \rangle}{d\omega}, \quad (11)$$

which is obtained under the assumption $\langle L_x \rangle \simeq L$. For the exact energy levels $E(L)$, dynamical MOI and the corresponding rotational frequencies are calculated from [7]

$$= \hbar^2 \left[\frac{d^2 E(L)}{dL^2} \right]^{-1} \simeq \frac{4\hbar^2}{E(L+2) - 2E(L) + E(L-2)},$$

$$\omega = \frac{1}{4\hbar} [E(L+2) - E(L-2)]. \quad (12)$$

Evolution of triaxiality with rotation is studied using the following expressions for the collective shape variable γ:

$$\tan \gamma = \sqrt{2} \frac{\langle Q_2 \rangle}{\langle Q_0 \rangle}, \quad (13)$$

$$\cos 3\gamma = -\sqrt{\frac{7}{2}} \frac{\langle Q \cdot Q \cdot Q \rangle}{\langle Q \cdot Q \rangle^{3/2}}. \quad (14)$$

The one-body expectation values of the quadrupole operator in Eq. (13) follow from Eq. (8) as $\langle Q_\mu \rangle = N A_{2\mu}$. The two-body expectation value in Eq. (14) is given in Eq. (7) and the three-body part is derived in Appendix. Equation (13) gives the average value for γ while Eq. (14) probes its fluctuations from this average. Thus the information content of the two expressions for γ are different and they compliment each other.

III. CRANKING IN THE sd-IBM

In this section, we perform cranking calculations for a variety of sd-IBM Hamiltonians and compare the results for the dynamical MOI and γ with the exact ones obtained from dynamical symmetries [SU(3) and O(6)], and from numerical diagonalization. For this purpose, we use a simple Hamiltonian with a quadrupole interaction and d-boson energy

$$H = -\kappa Q \cdot Q + \varepsilon \hat{n}_d. \quad (15)$$

Following the convention, we denote the parameters of the quadrupole operator by $t_{202} = 1$ and $t_{222} = \chi$. The SU(3) limit

is obtained when $\varepsilon=0$ and $\chi=-\sqrt{7}/2$, and the O(6) limit when $\varepsilon=\chi=0$. To test more realistic Hamiltonians, we use the middle value for χ ($-\sqrt{7}/4$), which leads to a better description of electromagnetic properties [8]. Inclusion of the d-boson energy with $\varepsilon=1.5N\kappa$ improves, in addition, the moment of inertia systematics [9]. The exact energy eigenvalues $E(L)$ are obtained from the Casimir operators in the case of the dynamical symmetries, and by numerical diagonalization of the Hamiltonian in the latter two cases.

For convenience in the variational problem, we set $x_{00}=1$ and drop the subscript 2 from the quadrupole mean fields, i.e., $x_{2m}=x_m$. The normalization is then given by

$$\mathcal{N}=1+x_0^2+2x_1^2+2x_2^2. \tag{16}$$

The expectation value of the Hamiltonian (15), $E(\mathbf{x})=\langle N,\mathbf{x}|H|N,\mathbf{x}\rangle$, can be written from Eqs. (6), (7) as

$$E(\mathbf{x})=-\kappa[N(N-1)(A_{20}^2+2A_{22}^2)+5\langle\hat{n}_s\rangle+(\chi^2+1)\langle\hat{n}_d\rangle]$$
$$+\varepsilon\langle\hat{n}_d\rangle. \tag{17}$$

Here the quadratic forms $A_{2\mu}$ follow from Eq. (8) as

$$A_{20}=\frac{1}{\mathcal{N}}[2x_0-\sqrt{2/7}\chi(x_0^2+x_1^2-2x_2^2)],$$

$$A_{22}=\frac{1}{\mathcal{N}}[2x_2+\sqrt{2/7}\chi(2x_0x_2+\sqrt{3/2}x_1^2)], \tag{18}$$

and the expectation values of $\hat{n}_s$ and $\hat{n}_d$ are

$$\langle\hat{n}_s\rangle=\frac{N}{\mathcal{N}}, \quad \langle\hat{n}_d\rangle=\frac{N}{\mathcal{N}}(x_0^2+2x_1^2+2x_2^2). \tag{19}$$

From Eq. (10), the cranking term is given by

$$\langle\hat{L}_x\rangle=\frac{2N}{\mathcal{N}}x_1(\sqrt{6}x_0+2x_2). \tag{20}$$

In Fig. 1, we compare the cranking results for the dynamical MOI obtained from Eq. (11) with those obtained from Eq. (12) using the exact energy levels for $N=10$ bosons. In the SU(3) and O(6) limits, the MOI is constant and given by $\mathcal{J}_{ex}^{(2)}=4/3\kappa=200/3$ and $2/\kappa=100$ $\hbar^2$/MeV, respectively. Note that both results are independent of N, and the constancy of MOI simply follows from the fact that $E(L)$ is quadratic in L in both cases. The SCC leads to a constant MOI in the SU(3) limit, as expected from a rigid rotor, but deviates from the exact result by about 5%. The O(6) limit corresponds to a γ-unstable rotor for which cranking is not expected to work well. Not surprisingly, comparison of the cranking results for $\mathcal{J}^{(2)}$ in Fig. 1 indicate a maximum deviation ($\sim 10\%$) from the exact result, as well as a small frequency dependence in MOI. We will comment on these deviations further when discussing the N dependence of the results below. The case with $\chi=-\sqrt{7}/4$ falls in between the two dynamical symmetry results. The dynamical MOI in-
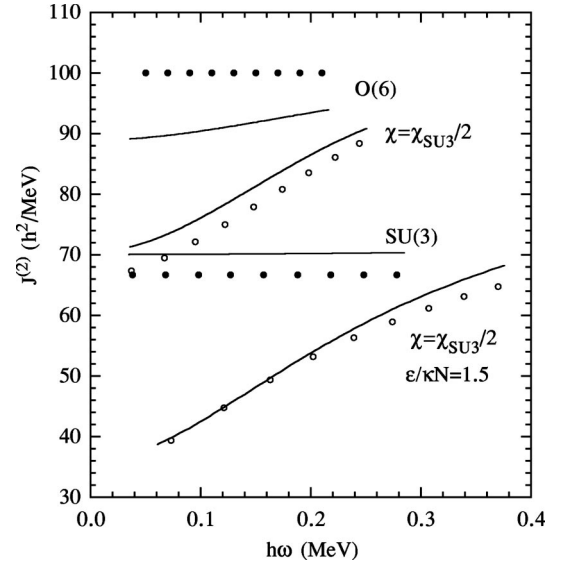
FIG. 1. Comparison of the cranking calculations of the dynamical moment of inertia in the sd-IBM (lines) with the exact results obtained from the dynamical symmetries SU(3) and O(6) (filled circles), and numerical diagonalization ($\chi=-\sqrt{7}/4$ with $\varepsilon=0$ and $\varepsilon=1.5N\kappa$) (open circles). In all cases, $N=10$ and $\kappa=-20$ keV are used.

creases with ω as in a typical deformed nucleus (Fig. 1), though the overall magnitude is still too large. The deviation between the cranking and the exact results in this case is comparable to that in the SU(3) limit, with the error getting smaller at higher frequencies. When a d-boson energy with $\varepsilon=1.5N\kappa$ is included in the Hamiltonian, which fits the observed range of MOI data better, the agreement between the cranking and exact results improve markedly, especially at lower frequencies.

The SCC is a semiclassical theory and it would be exact in the classical limit when $N\to\infty$. Thus to understand the nature of discrepancies seen in Fig. 1 better, we need to study the N dependence of the results. In Fig. 2, we show the SCC results for $\mathcal{J}^{(2)}$ as a function of N in the SU(3) and O(6) limits. Since the MOI is not constant in the O(6) limit, we have taken the value of $\mathcal{J}^{(2)}$ at the middle-frequency for each N. The curves that trace the SCC results are obtained from

$$\mathcal{J}_{cr}^{(2)}=\mathcal{J}_{ex}^{(2)}\left(1+\frac{1}{2N}+\frac{1}{7N^2}\right), \tag{21}$$

in the SU(3) limit, and from

$$\mathcal{J}_{cr}^{(2)}=\mathcal{J}_{ex}^{(2)}\left(1-\frac{1}{N}+\frac{1}{2N^2}\right), \tag{22}$$

in the O(6) limit. The coefficients in Eqs. (21) and (22) are derived from a $1/N$ expansion of the SCC equation (1). It is clear from Fig. 2 and Eqs. (21), (22) that the SCC calculation of $\mathcal{J}^{(2)}$ is correct to leading order but fails in higher orders in $1/N$ by generating spurious correction terms. A comparison of Eq. (17) with the accurate angular-momentum-projected result [5] confirms that the incorrect treatment of the $1/N$
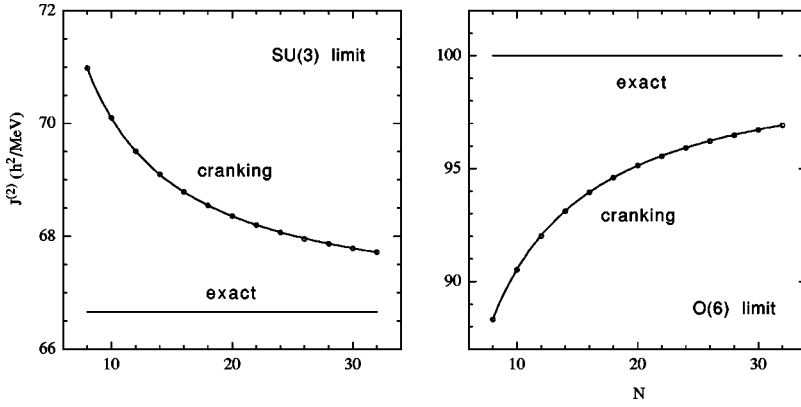
FIG. 2. Boson number dependence of the cranking dynamical moment of inertia in the SU(3) and O(6) limits of the sd-IBM (circles). The lines that trace the circles are obtained from Eq. (21) in the SU(3) case and from Eq. (22) in the O(6) case.

terms in the SCC is the cause of the discrepancy. It is interesting to note that an agreement is obtained if one uses the Casimir operator of the SU(3) given by $C_2 = Q \cdot Q + (3/8)L \cdot L$, instead of just $Q \cdot Q$. In this case, the incorrect $1/N$ contribution from the $Q \cdot Q$ interaction is exactly canceled by the spurious contribution from the $L \cdot L$ term. Another interesting observation is that the best agreement of SCC with the exact results is achieved in the realistic case with $\chi = -\sqrt{7}/4$ and $\varepsilon = 1.5N\kappa$. This happens because the $1/N$ term is now dominated by the leading contribution from $\langle \hat{n}_d \rangle$, which is correctly treated in the SCC. The errors from $\langle \hat{n}_d \rangle$ contribute at the $1/N^2$ level, and these become apparent only at the high-rotational frequencies as is apparent in Fig. 1.

We next study the effects of triaxiality in SCC. It is well known that the energy surface of an sd-IBM Hamiltonian with one- and two-body interactions has an axially symmetric minima in the deformed phase [10]. An exception occurs in the O(6) limit, where a γ-unstable shape develops. The SCC calculations in the O(6) limit give 30° for both the average γ (13) and its fluctuations (14) at all frequencies. Thus the SCC results are consistent with the description of the O(6) limit using a triaxial intrinsic state with $\gamma = 30^\circ$, which has a very shallow minimum in the γ direction [11]. Frequency independence of the results corroborates with the

fact that the O(6) states remain γ unstable at all spins. In Fig. 3, we show the evolution of the triaxiality angle γ with the cranking frequency for the remaining three cases discussed above for three different boson numbers, $N = 10$, 15, 20. Results obtained from both Eqs. (13) (solid line) and (14) (dashed line) are shown. The ground band in the SU(3) limit can be described exactly by angular momentum projection from an axially symmetric intrinsic state, therefore, both average γ and its fluctuations should vanish at *all* frequencies. The SCC results (Fig. 3, left) start with $\gamma = 0$ at low ω but deviate from it systematically with increasing frequency. Although the situation appears to be improving with increasing N, similar to the case in $\mathcal{J}^{(2)}$, in fact, this is merely due to the extension of the spectrum with N ($\omega_{max} \propto N$). If one scales out the N dependence (i.e., plots γ against ω/N), then all the curves with different N overlap. Thus γ can be written as a power expansion in ω/N with the leading (N independent) term being zero. This situation is similar to that encountered in the study of $\mathcal{J}^{(2)}$: the SCC gets the leading order term correctly ($\gamma = 0$) but fails in higher-orders in $1/N$ by generating spurious terms in powers of ω/N. The fact that the incorrect $1/N$ terms in γ all depend on the cranking frequency makes the SCC results increasingly unreliable at higher frequencies. The onset of triaxiality observed at around midfrequency ($\omega_{max}/2$) in all curves in Fig. 3 is thus
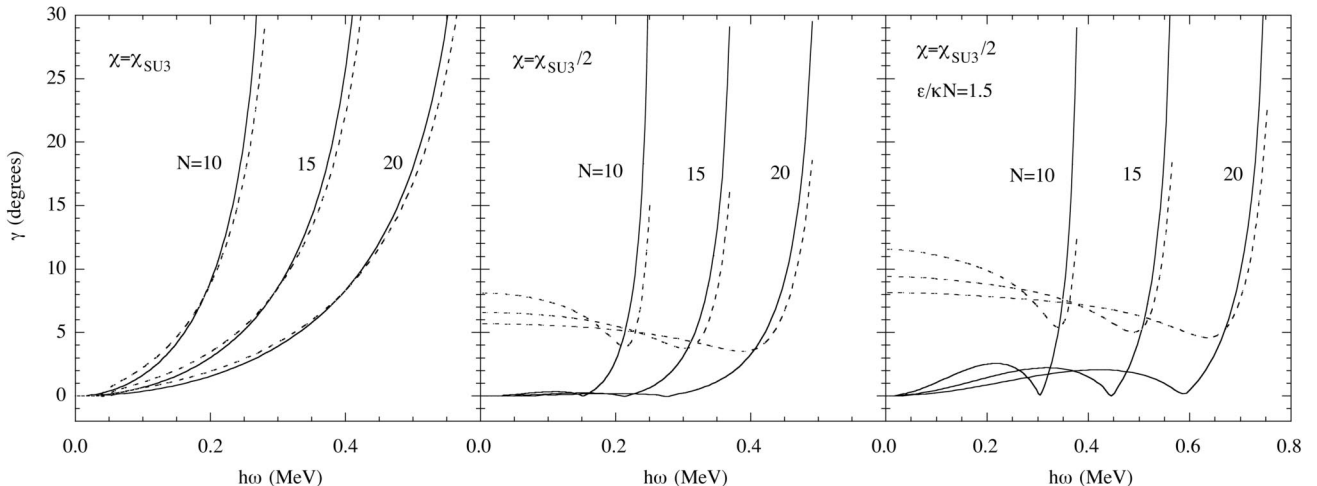
FIG. 3. Cranking calculations of the triaxiality angle γ in the sd-IBM for the three cases shown in Fig. 1 for $N = 10$, 15, 20. The solid lines indicate average γ obtained from Eq. (13) and the dashed lines correspond to its fluctuations given by Eq. (14).

due the failure of the SCC and not a genuine feature of the boson system. We remark that despite the sudden increase in the calculated γ values, $\mathcal{J}^{(2)}$ remains constant in the SU(3) limit, suggesting that triaxiality has a negligible effect on MOI in the interacting boson model.

We interpret the remaining more realistic cases in the light of the SU(3) test. In the case of $\chi = -\sqrt{7}/4$ (Fig. 3, middle), the average γ (solid lines) remains around zero except at high frequencies. Attributing this sudden rise in γ to the break down of SCC, we see that $\gamma \sim 0$ for all ground-band states of a $Q \cdot Q$ Hamiltonian. The fluctuations (dashed lines), on the other hand, are nonzero but get smaller with increasing N. The values of fluctuations at $\omega = 0$ are consistent with those obtained from an exact calculation for the ground state [12]. At higher frequencies there is a small reduction in fluctuations, that is, rotations have a slightly stabilizing effect on the γ motion. Increasing the boson number also suppresses fluctuations, which is due to the energy surface becoming deeper in the γ direction with larger N values. The last case with $\varepsilon = 1.5N\kappa$ (Fig. 3, right) has broadly the same features. The one-body term cannot induce triaxiality alone, therefore, the small deviation in average γ from zero at midfrequencies is presumably due to errors in SCC. There is an increase in fluctuations compared to the middle panel, which can be explained as due to the energy surface becoming shallower with the addition of the one-body term. These results indicate that rotations have a rather limited effect on the shape variables in the sd-IBM, with average γ remaining nearly constant at zero, and its fluctuations being slightly reduced from the ground state value at higher spins.

IV. CRANKING IN THE sdg-IBM

In contrast to the sd-IBM, where numerical diagonalization is a routine task, the sdg-IBM already suffers from the large basis problem, and exact diagonalization is not possible for $N > 11$, that is, for most of the deformed nuclei. The $1/N$ expansion circumvents this problem but because it assumes axial symmetry, one cannot use it to address questions on triaxiality. Here we perform cranking calculations in the sdg-IBM to study the evolution of shapes with rotation without restriction to axial symmetry. For the Hamiltonian, we choose

$$H = -\kappa_2 Q \cdot Q - \kappa_4 T_4 \cdot T_4 + \varepsilon_d \hat{n}_d + \epsilon_g \hat{n}_g, \quad (23)$$

which has been shown to provide a good representation of data in rare-earth and actinide nuclei [13]. As in Sec. III, we set $q_{02} = h_{02} = 1$ and $x_{00} = 1$. Then the normalization is given by

$$\mathcal{N} = 1 + x_{20}^2 + 2x_{21}^2 + 2x_{22}^2 + x_{40}^2 + 2x_{41}^2 + 2x_{42}^2 + 2x_{43}^2 + 2x_{44}^2. \quad (24)$$

The expectation value of the Hamiltonian (23) follows from Eqs. (6), (7) as

$$E(\mathbf{x}) = -\kappa_2[N(N-1)(A_{20}^2 + 2A_{22}^2) + 5\langle \hat{n}_s \rangle + (1 + q_{22}^2 + q_{24}^2) \\ \times \langle \hat{n}_d \rangle + (5/9)(q_{24}^2 + q_{44}^2)\langle \hat{n}_g \rangle] - \kappa_4[N(N-1)(A_{40}^2 \\ + 2A_{42}^2 + 2A_{44}^2) + 9\langle \hat{n}_s \rangle + (9/5)(h_{22}^2 + h_{24}^2)\langle \hat{n}_d \rangle \\ + (1 + h_{24}^2 + h_{44}^2)\langle \hat{n}_g \rangle] + \varepsilon_d \langle \hat{n}_d \rangle + \varepsilon_g \langle \hat{n}_g \rangle. \quad (25)$$

Here the quadrupole quadratic forms $A_{2\mu}$ are given by

$$A_{20} = \frac{1}{\mathcal{N}}[2x_{20} - \sqrt{2/7}q_{22}(x_{20}^2 + x_{21}^2 - 2x_{22}^2) \\ + 2\sqrt{2/21}q_{24}(\sqrt{3}x_{20}x_{40} + \sqrt{10}x_{21}x_{41} + \sqrt{5}x_{22}x_{42}) \\ - (1/3\sqrt{77})q_{44}(10x_{40}^2 + 17x_{41}^2 + 8x_{42}^2 - 7x_{43}^2 - 28x_{44}^2)],$$

$$A_{22} = \frac{1}{\mathcal{N}}[2x_{22} + \sqrt{2/7}q_{22}(2x_{20}x_{22} + \sqrt{3/2}x_{21}^2) \\ + (2/3\sqrt{14})q_{24}(x_{22}x_{40} + \sqrt{5}x_{21}x_{41} + \sqrt{15}x_{20}x_{42} \\ + \sqrt{35}x_{21}x_{43} + \sqrt{70}x_{22}x_{44}) + \sqrt{2/33}q_{44} \\ \times (2x_{42}x_{44} + 3x_{41}x_{43} + 3\sqrt{10/7}x_{40}x_{42} + (5/\sqrt{7})x_{41}^2)], \quad (26)$$

and the hexadecapole quadratic forms $A_{4\mu}$ by

$$A_{40} = \frac{1}{\mathcal{N}}[2x_{40} + \sqrt{2/35}h_{22}(3x_{20}^2 - 4x_{21}^2 + x_{22}^2) \\ - (2/\sqrt{77})h_{24}(2\sqrt{5}x_{20}x_{40} + \sqrt{6}x_{21}x_{41} - 6\sqrt{3}x_{22}x_{42}) \\ + \sqrt{2/1001}h_{44}(9x_{40}^2 + 9x_{41}^2 - 11x_{42}^2 - 21x_{43}^2 + 14x_{44}^2)],$$

$$A_{42} = \frac{1}{\mathcal{N}}[2x_{42} + (1/\sqrt{7})h_{22}(\sqrt{6}x_{20}x_{22} - 2x_{21}^2) + \sqrt{3/385}h_{24} \\ \times (6\sqrt{5}x_{22}x_{40} + 9x_{21}x_{41} - (8/\sqrt{3})x_{20}x_{42} - 5\sqrt{7}x_{21}x_{43} \\ + 2\sqrt{14}x_{22}x_{44}) + \sqrt{5/1001}h_{44}(6\sqrt{7}x_{42}x_{44} + 2\sqrt{7}x_{41}x_{43} \\ - 11x_{40}x_{42} - 6x_{41}^2)],$$

$$A_{44} = \frac{1}{\mathcal{N}}[2x_{44} + h_{22}x_{22}^2 + (2/\sqrt{55})h_{24}(\sqrt{6}x_{22}x_{42} + \sqrt{21}x_{21}x_{43} \\ + 2\sqrt{7}x_{20}x_{44}) + (1/\sqrt{143})h_{44}(2\sqrt{14}x_{40}x_{44} \\ + 2\sqrt{35}x_{41}x_{43} + 3\sqrt{5}x_{42}^2)]. \quad (27)$$

The one-body expectation values in Eq. (25) are given by Eq. (19) and

$$\langle \hat{n}_g \rangle = \frac{N}{\mathcal{N}}(x_{40}^2 + 2x_{41}^2 + 2x_{42}^2 + 2x_{43}^2 + 2x_{44}^2). \quad (28)$$

Finally, from Eq. (10) the cranking term is

$$\langle \hat{L}_x \rangle = \frac{2N}{\mathcal{N}} [x_{21}(\sqrt{6}x_{20}+2x_{22}) + x_{41}(2\sqrt{5}x_{40}+3\sqrt{2}x_{42})$$

$$+ x_{43}(\sqrt{14}x_{42}+2\sqrt{2}x_{44})]. \tag{29}$$

In view of the numerous parameters in the sdg-IBM, we limit our discussion to a realistic range tailored to data [13]. Accordingly, the quadrupole parameters $\{q_{22},q_{24},q_{44}\}$ are scaled from their SU(3) values with a single factor q as suggested by microscopics [14]. The hexadecapole parameters $\{h_{22},h_{24},h_{44}\}$ are determined from those of q_{jl} through the commutation condition

$$[\bar{h},\bar{q}]=0, \quad \bar{q}_{jl}=\langle j0l0|20\rangle q_{jl}, \quad \bar{h}_{jl}=\langle j0l0|40\rangle h_{jl}, \tag{30}$$

which reproduce the available $E4$ data reasonably well [13]. We adapt the realistic sd-IBM parameters used in Fig. 1, $\kappa_2=-20$ keV, $q=0.5$ and $\epsilon_d=1.5N\kappa_2$, and use further, $\epsilon_g=4N\kappa_2$ and $\kappa_4/\kappa_2=0$–0.4. Energy levels are very well described in the sdg-IBM [13], therefore we do not dwell on a study of MOI apart from noting that all the SCC calculations of $\mathcal{J}^{(2)}$ exhibit the characteristic rise with increasing frequency seen in experimental spectra. We focus instead on the shape question which could not be addressed in the $1/N$ expansion approach. With the parameter set described above, the SCC calculations of γ in the sdg-IBM are very similar to those of the sd-IBM with the realistic set of parameters (Fig. 3, right). Because the hexadecapole interaction is a relatively novel feature not used in the sd-IBM, we briefly comment on its effect. Inclusion of the hexadecapole interaction does not cause any deviation from the axial shape but depending on its sign, it either decreases the fluctuations in γ (attractive) or increases them (repulsive) by a few degrees. This is very similar to the effect of changing the strength of the quadrupole interaction, in that, a larger κ_2 leads to a deeper energy well in the γ direction, therefore reduces the fluctuations, and vice versa. In certain parametrizations where the boson energies are neglected, it is possible to obtain nonaxial shapes in the sdg-IBM [15]. However, once a g-boson energy of $\epsilon_g \sim 1$ MeV is included, as demanded by the experimental spectra, such deviations from axial symmetry quickly disappear. In short, the congruence found between the sd- and sdg-IBM results with regard to the shape variable γ is a direct consequence of the fairly high g-boson energy, which limits the effect of g bosons to a perturbative range at low to medium spins.

V. CONCLUSIONS

We have tested the self-consistent cranking method using the exact IBM results obtained from dynamical symmetries and numerical diagonalization. The SCC results for the dynamic MOI are in good agreement with the exact ones, especially in realistic cases where the deviation is at most a few percent. The study of shapes using SCC, on the other hand, remains problematic due to the generation of spurious frequency-dependent terms in shape variables, which become dominant at high frequencies. Nevertheless, SCC can give reliable information on evolution of shapes in the low to mid frequency range. Our study of shapes using SCC indicates that both the sd- and sdg-IBM with one- and two-body interactions retain the axial shape ($\gamma=0$) with fluctuations around 10°, as long as the model parameters are restricted to a realistic range that reproduce the data. The only frequency dependence in shape variables is observed in the fluctuations in γ which is slightly reduced with increasing frequency. These results suggest that if the triaxial effects are important and need to be included in the IBM, then the remedy should be sought in three-body interactions rather than g bosons.

APPENDIX: THREE-BODY OPERATORS

Here we derive the expectation value of the three-body quadrupole interaction in Eq. (14). The scalar product of the three quadrupole operators is defined as

$$Q \cdot Q \cdot Q = [QQ]^{(2)} \cdot Q. \tag{A1}$$

The expectation value of this three-body term in the condensate state Eq. (2) is given by

$$\langle Q \cdot Q \cdot Q \rangle = \frac{1}{N!} \sum_{\mu_1\mu_2\mu} (-1)^\mu \langle 2\mu_1 2\mu_2|2\mu\rangle$$
$$\times \langle 0|b^N Q_{\mu_1}Q_{\mu_2}Q_{-\mu}(b^\dagger)^N|0\rangle. \tag{A2}$$

Writing the quadrupole operators explicitly and commuting all the boson creation operators to the left, one obtains a three-body term, three two-body terms, and a one-body term. Using boson calculus, the matrix elements of these normal ordered operators can be evaluated in a straightforward manner with the result

$$\langle Q \cdot Q \cdot Q \rangle = \sum_{\mu_1\mu_2\mu} (-1)^\mu \langle 2\mu_1 2\mu_2|2\mu\rangle \sum_{\substack{j_1j_2j_3l_1l_2l_3 \\ m_1m_2m_3n_1n_2n_3}} (-1)^{n_1+n_2+n_3} q_{j_1l_1}q_{j_2l_2}q_{j_3l_3} \times \langle j_1m_1l_1n_1|2\mu_1\rangle \langle j_2m_2l_2n_2|2\mu_2\rangle$$

$$\times \langle j_3m_3l_3n_3|2-\mu\rangle \times \{N(N-1)(N-2)x_{j_1m_1}x_{j_2m_2}x_{j_3m_3}x_{l_1-n_1}x_{l_2-n_2}x_{l_3-n_3}$$

$$+ N(N-1)[x_{j_1m_1}x_{j_2m_2}x_{l_2-n_2}x_{l_3-n_3}\delta_{j_3l_1}\delta_{m_3-n_1} + x_{j_1m_1}x_{j_2m_2}\times x_{l_1-n_1}x_{l_3-n_3}\delta_{j_3l_2}\delta_{m_3-n_2}$$

$$+ x_{j_1m_1}x_{j_3m_3}x_{l_2-n_2}x_{l_3-n_3}\delta_{j_2l_1}\delta_{m_2-n_1}] + Nx_{j_1m_1}x_{l_3-n_3}\delta_{j_2l_1}\delta_{m_2-n_1}\delta_{j_3l_2}\delta_{m_3-n_2}\}. \tag{A3}$$

The three-body part (the first term) is seen to involve a triple product of the one-body expectation values $A_{2\mu}$ defined in Eq. (8). In the effective two-body terms, three C-G coefficients can be summed to yield a 6-j symbol and a C-G coefficient. After some manipulations of the summation indices, all 3 terms can be shown to be equivalent. Finally, the sum of the four C-G coefficients in the effective one-body term gives a 6-j symbol. Thus, Eq. (A3) can be written compactly as

$$\langle Q \cdot Q \cdot Q \rangle = N(N-1)(N-2)$$

$$\times \sum_{\mu_1 \mu_2 \mu} (-1)^\mu \langle 2\mu_1 2\mu_2 | 2\mu \rangle A_{2\mu_1} A_{2\mu_2} A_{2-\mu}$$

$$+ 3N(N-1) \sum_\mu (-1)^\mu \tilde{A}_{2\mu} A_{2-\mu}$$

$$+ N \sum_{lm} \tilde{\varepsilon}_l x_{lm}^2, \qquad (A4)$$

where we have introduced

$$\tilde{q}_{jl} = 5 \sum_i (-1)^{i+j+l} \begin{Bmatrix} j & l & 2 \\ 2 & 2 & i \end{Bmatrix} q_{ji} q_{il},$$

$$\tilde{\varepsilon}_l = \frac{25}{2l+1} \sum_{ij} \begin{Bmatrix} l & i & 2 \\ 2 & 2 & j \end{Bmatrix} q_{li} q_{ij} q_{jl}, \qquad (A5)$$

and $\tilde{A}_{2\mu}$ is obtained from $A_{2\mu}$ by replacing $q_{jl} \to \tilde{q}_{jl}$ in Eq. (8). Note that symmetry of q_{jl} is retained, i.e., $\tilde{q}_{jl} = \tilde{q}_{lj}$. Using the fact that $A_{21} = A_{2-1} = 0$ and $A_{22} = A_{2-2}$, the sums in Eq. (A4) involving $A_{2\mu}$ can be carried out to yield

$$\langle Q \cdot Q \cdot Q \rangle = N(N-1)(N-2) \sqrt{2/7} (-A_{20}^2 + 6A_{22}^2) A_{20}$$

$$+ 3N(N-1) \tilde{A}_{20} A_{20} + 2 \tilde{A}_{22} A_{22} + N \sum_{lm} \tilde{\varepsilon}_l x_{lm}^2. \qquad (A6)$$

In the case of the sd-IBM, A_{20} and A_{22} are given in Eq. (18). The contracted parameters in Eq. (A5) become

$$\tilde{q}_{02} = \chi, \quad \tilde{q}_{22} = 1 - 3\chi^2/14,$$

$$\tilde{\varepsilon}_0 = 5\chi, \quad \tilde{\varepsilon}_2 = 2\chi - 3\chi^3/14. \qquad (A7)$$

Using these values of $\tilde{q}_{jl}$, one obtains for $\tilde{A}_{20}$ and $\tilde{A}_{22}$

$$\tilde{A}_{20} = \frac{1}{\mathcal{N}} [2\chi x_0 - \sqrt{2/7}(1-3\chi^2/14)(x_0^2 + x_1^2 - 2x_2^2)],$$

$$\tilde{A}_{22} = \frac{1}{\mathcal{N}} [2\chi x_2 + \sqrt{2/7}(1-3\chi^2/14)(2x_0 x_2 + \sqrt{3/2} x_1^2)]. \qquad (A8)$$

In the sdg-IBM, these parameters are given by

$$\tilde{q}_{02} = q_{22}, \quad \tilde{q}_{22} = 1 - \frac{3}{14} q_{22}^2 + \frac{2}{7} q_{24}^2,$$

$$\tilde{q}_{24} = \frac{2}{7} q_{22} q_{24} - 5 \sqrt{\frac{22}{42}} q_{24} q_{44},$$

$$\tilde{q}_{44} = 5 \sqrt{\frac{22}{42}} q_{24}^2 - \frac{65}{42\sqrt{22}} q_{44}^2,$$

$$\tilde{\varepsilon}_0 = 5 q_{22}, \quad \tilde{\varepsilon}_2 = 2 q_{22} - \frac{3}{14} q_{22}^3 + \frac{4}{7} q_{22} q_{24}^2 + 5 \sqrt{\frac{22}{42}} q_{24}^2 q_{44},$$

$$\tilde{\varepsilon}_4 = \frac{10}{63} q_{22} q_{24}^2 + \frac{25\sqrt{22}}{189} q_{24}^2 q_{44} - \frac{325}{378\sqrt{22}} q_{44}^3. \qquad (A9)$$

[1] P. Ring and P. Schuck, *The Nuclear Many-Body Problem* (Springer-Verlag, New York, 1980).
[2] C. Baktash, B. Haas, and W. Nazarewicz, Annu. Rev. Nucl. Part. Sci. **45**, 485 (1995).
[3] F. Iachello and A. Arima, *The Interacting Boson Model* (Cambridge University Press, Cambridge, 1987).
[4] H. Schaaser and D. M. Brink, Phys. Lett. **14B**, 269 (1984); Nucl. Phys. **A452**, 1 (1986).
[5] S. Kuyucak and I. Morrison, Ann. Phys. (N.Y.) **181**, 79 (1988); **195**, 126 (1989).
[6] S. Aberg, H. Flocard, and W. Nazarewicz, Annu. Rev. Nucl. Part. Sci. **40**, 439 (1990).
[7] A. Bohr and B. R. Mottelson, Phys. Scr. **24**, 71 (1981).
[8] R. F. Casten and D. D. Warner, Rev. Mod. Phys. **60**, 389 (1988).
[9] S. Kuyucak and S. C. Li, Phys. Lett. B **354**, 189 (1995).
[10] J. N. Ginocchio and M. W. Kirson, Nucl. Phys. **A350**, 31 (1980).
[11] T. Otsuka and M. Sugita, Phys. Rev. Lett. **59**, 1541 (1987).
[12] J. P. Elliott, J. A. Evans, and P. Van Isacker, Phys. Rev. Lett. **57**, 1124 (1986).
[13] S. C. Li and S. Kuyucak, Nucl. Phys. **A604**, 305 (1996).
[14] T. Otsuka, A. Arima, and F. Iachello, Nucl. Phys. **A309**, 1 (1978).
[15] S. Kuyucak and I. Morrison, Phys. Lett. B **255**, 305 (1991).